

One-dimensional analytical model for optimizing porosity distribution of multi-layered electrode in redox flow cells

Junyi Tao¹, Zhichao Chen¹, Limin Qi¹, Menglian Zheng^{1,2*}

¹ School of Energy Engineering, Zhejiang University, Hangzhou, China

² Institute of Thermal Science and Power Systems, School of Energy Engineering, Zhejiang University, Hangzhou, China
(Corresponding Author)

ABSTRACT

The multi-layered electrode is expected to exhibit improved flow battery performance due to its variable flow and electrochemical properties that can be locally optimized in different layers. The porosity combination and the thickness of layers with different porosities will affect the reaction rate and the uniformity of the reactant distribution. Although a variety of models have been developed to guide the design of the electrode microstructure, how to mathematically optimize the properties of the electrode with multi-layered carbon paper sheets, remains unknown. In the present study, the authors devise a 3D, multi-physical vanadium redox flow battery model with the multi-layered electrode, and put forward a 1D analytical model for optimizing porosity distribution of multi-layered electrode in the redox flow cell. The optimization results based on the 3D simulations are presented.

Keywords: redox flow battery, VRFB, porous material electrode, multi-layered electrode, porosity distribution, analytical model

NONMENCLATURE

Abbreviations

RFB	Redox flow battery
VRFB	Vanadium redox flow battery

Symbols

U	Total overpotential
I_{app}	Applied charge/discharge current
ΔP_{pipe}	Electrolyte pressure loss in pipes

ΔP	Electrolyte pressure loss within electrode
Q	Applied flow rate
μ	Electrolyte dynamic viscosity
h_{ed}	Height of electrode
A_{ed}	Cross-sectional area of electrode
d_f	Mean fiber diameter of electrode
ε	Porosity of electrode
λ_{CK}	Carman-Kozeny constant
κ	Liquid phase conductivity
σ	Solid phase conductivity
a	Specific surface area
i_0	Exchange current density
n	Electron transfer number
F	Faraday's constant
k_B	Boltzmann constant
T	Temperature

1. INTRODUCTION

Redox flow batteries (RFBs) have been regarded as one of the most promising electrochemical energy storage technologies for commercialization, owing to their desirable characteristics such as cost-effectiveness especially when they are used as long-duration storage, great ease for maintenance and thermal management, and relatively long lifetime. These features are inherent to the unique architecture of redox flow batteries that store electrolytes in external tanks and circulate electrolytes through flow cells upon charge and discharge. Such architecture requires porous electrodes to maintain good mass transfer capabilities and provide

sufficient active sites while at relatively low expenses with respect to hydraulic losses.

Over the past few years, carbon felt, carbon paper, and carbon cloth are widely used and investigated as electrodes in redox flow cells. Among them, carbon paper and carbon cloth have gained rising attentions because of their superiority in terms of conductivity. With the zero-gap flow cell design proposed by Aaron et al. [1], stacked sheets of carbon paper were assembled and fit into the cell stack smoothly, leading to significantly increases in the peak power density of a vanadium redox flow battery (VRFB) and significant reductions in the battery system cost. Recognizing that the peak power density of flow cells with carbon paper-based electrodes typically suffer from limited active sites within carbon paper media, multiple sheets of carbon paper are usually compressed together to form a multi-layered electrode. By using the non-zero gap structure, Houser et al. [2] varied the number of layered sheets and found that the effects depend on the condition of the flow field. For example, the increase in the number of sheets from 3 to 5 marginally affected the resulting polarization curves under the condition of the interdigitated flow field, while led to a significant increase in the maximum current density under the condition of the serpentine flow field [2]. In addition to the number of layered sheets, the properties, such as porosity, of carbon paper sheets also significantly affect the performance of the flow cell. Along with the penetration of electrolytes into the porous material in the through-plane direction and the flow of electrolytes from the inlet to the outlet of the cell, the concentrations of active species are unevenly distributed within the electrode, making it necessary the properties of the electrode being tuned with the concentration distribution. For example, Chen et al. [3] studied the two-dimensional electrode with variable porosities and compared the situations of step increase, step decrease, linear increase of the porosity in the through-plane direction. Yoon et al. [4] proposed to vary the local porosity of the electrode from the inlet to the outlet, and pointed out that changing the electrode porosity at the inlet was more effective than changing it at the outlet.

To this end, it is essential to optimize the local porosity of the electrode in the redox flow cell by taking into account the synergies of the number of the layered sheets, the design of the flow field, and the unevenly distributed concentration of active species within the electrode. Furthermore, when the 3D printing technology becomes mature and practical for printing

heterogeneous carbon-fiber-based porous material (e.g., [5][6]), how to mathematically optimize the pore

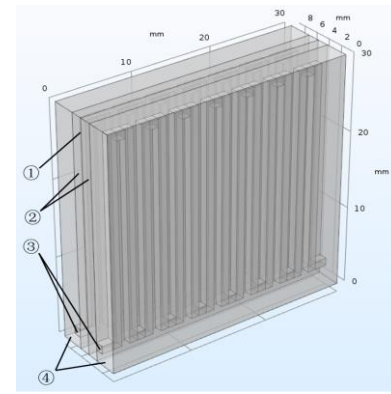


Fig 1 Geometry of the VRFB flow cell. ① membrane, ② electrodes, ③ flow channels for serpentine flow field, and ④ bipolar plates.

structure and properties, especially local properties, has become of rising importance. Although a variety of models, such as COMSOL, pore-network and Lattice Boltzmann method-based models, have been developed to guide the design of the electrode microstructure, how to mathematically optimize the properties of the electrode with multi-layered carbon paper sheets, remains unknown. In order to further explore the improvement effect of the porosity distribution on the performance of VRFB, the present study first establishes a multi-physical, three-dimensional VRFB flow cell model, and then investigates the impacts of varying porosity combinations in the through-plane direction of the flow cell on the resulting average velocity and concentration of active species. An analytical one-dimensional model analytical model is developed, which is expected to be used to optimize the local porosity of the electrode.

2. METHODS

2.1 3D multi-physical model

The 3D multi-physical model is first developed for the VRFB flow cell, which is mainly composed of two bipolar plates with flow channels carved, two electrodes, and one ion-selective membrane. The geometry of the flow cell is illustrated in Fig. 1. The size of the electrode is set as 30 mm*30 mm and the serpentine flow field is applied with the width and height of the channel and rib all corresponding to 1 mm. As shown in Fig. 2, the positive and negative electrodes are divided into five 0.3-mm-thick layers, respectively, along the direction

perpendicular to the membrane (i.e., in the through-plane direction). Different porosities can be applied to these layers to show the impacts of porosity variations in the through-plane direction on the overall performance of the VRFB. Three porosity candidates of 0.7, 0.82, and 0.89 are selected based on the typically properties of commercially available SGL carbon paper. By stacking five sheets of carbon paper with three different porosities, different electrodes are prepared for simulations. Note that the current version of one-dimensional model is based on a two-layered electrode. Therefore, in the 3D-model simulations, combinations of two rather three porosities are implemented for the five layers. Detailed combinations can be found in *Results*.

Based on the assumptions that the fluid is incompressible, the vanadium ions are dissolved in the dilute solution, and the electrode material is isotropic, the 3D model is developed by using the software .COMSOL Multiphysics 5.4. Governing equations with respect to the kinetics, electrochemical process, mass balance, and hydraulic process along with relevant parameters to describe the properties of components and processes within the flow cell are taken from Ref. [7]. The tolerance level of the simulation is set to below 0.1. The developed model is validated against experimental results taken from Ref. [7] (compared against the charge curve displayed in Fig. 3 of Ref. [7]). The deviations between the simulative and experimental results are within 7%, mainly due to the discrepancies between simulative and experimental parameters.

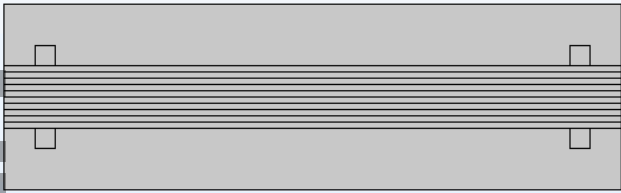


Fig 2 Illustration of the flow cell with 5-layered electrodes.

2.2 1D analytical model

To facilitate the optimization of the local porosity in the through-plane direction, the present study established a 1D analytical model to predict the total losses (pump losses included) under varying porosity combinations.

The function of the total losses is as below:

$$E_{loss} = UI_{app} + (\Delta P_{pipe} + \Delta P)Q \quad (1)$$

Where, U denotes the total overpotential under the applied current I_{app} , ΔP_{pipe} and ΔP denote the pressure drops of the electrolytes along the pipes and within the electrode, respectively, and the applied flow rate is Q .

Suppose that the pressure drops, flow rate and applied current are constant during the charge/discharge process. The total losses can be divided by the square of the applied current to form the resistance function as:

$$R_f = r_{net} + \frac{\Delta PQ}{I_{app}^2} = r_{net} + r_{flow} \quad (2)$$

The pressure drop of electrolytes can be described by the permeability of the porous electrode and the applied electrolyte flow rate as follows [8]:

$$\Delta P = \frac{\mu h_{ed}}{\lambda A_{ed}} \times Q \quad (3)$$

$$\lambda = \frac{d_f^2 \varepsilon^3}{\lambda_{CK} (1 - \varepsilon)^2} \quad (4)$$

Where, μ denotes the electrolyte dynamic viscosity, h_{ed} denotes the height of the electrode, λ denotes the porous electrode permeability, A_{ed} denotes the cross-sectional area of the electrode, d_f denotes the mean fiber diameter of the electrode, ε denotes the porosity of the porous electrode, and λ_{CK} denotes the Carman-Kozeny constant for the fibrous material.

The geometry of the 1D model is illustrated in Fig. 3. The electrode is divided into the electrode part in the solid phase and the electrolyte part in the liquid phase. The interface between the electrode and the membrane is assumed to be at $x = 0$. With the potentials in the solid phase and the liquid phase at the location x being defined as $\varphi_s(x)$ and $\varphi_l(x)$, respectively, and the current

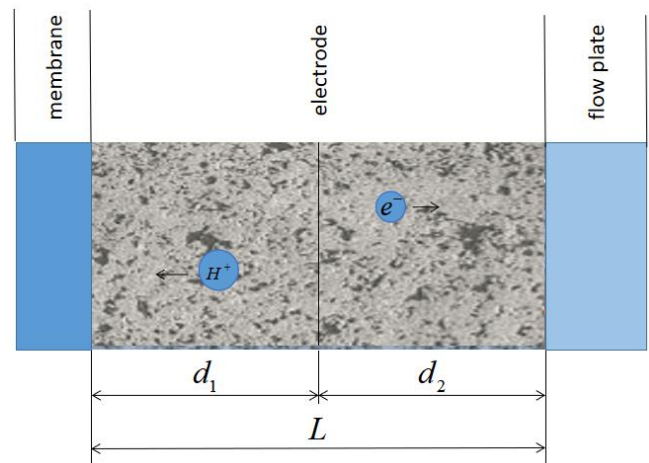


Fig 3 Geometry of the 1D analytical model. The electrode is divided into two parts with the thickness corresponding to d_1 and d_2 , respectively.

densities as $i_s(x)$ and $i_L(x)$, respectively, the governing equations are written as follows:

$$i_s(x) = -\sigma \frac{d\phi_s(x)}{dx} \quad (5)$$

$$i_L(x) = -\kappa \frac{d\phi_L(x)}{dx} \quad (6)$$

$$\frac{di_{app}}{dx} = 0 \quad (7)$$

$$i_s(x) + i_L(x) = i_{app} \quad (8)$$

The boundary conditions are as follows:

$$\begin{cases} x = 0: & i_L(x) = i_{app}, \phi_L(x) = 0 \\ x = L: & i_s(x) = i_{app} \end{cases} \quad (9)$$

Where, κ denotes the liquid phase conductivity (assumed to be independent from the position x) and σ denotes the solid phase conductivity. The latter equals σ_1 when $0 \leq x < d_1$ and σ_2 when $d_1 \leq x < L$.

Supposing the active species in VRFB possess rapid kinetics, the Butler-Volmer equation can be linearized as:

$$\frac{di_L(x)}{dx} = ai_0 \frac{nF}{k_B T} [\phi_s(x) - \phi_L(x)] \quad (10)$$

Where, a denotes the specific surface area of the electrode, i_0 denotes the exchange current density, n denotes the electron transfer number, F denotes Faraday's constant, k_B denotes Boltzmann constant, and T denotes the temperature.

After deriving x from both sides of the linearly simplified Butler-Volmer equation and combining Eqs. (5), (6), (7), and (8), the following second-order, heterogeneous linear differential equation is obtained:

$$\frac{d^2 i_L(x)}{dx^2} - \frac{ai_0 nF}{k\sigma k_B T} (\sigma + \kappa) i_L(x) + \frac{ai_0 nF}{k\sigma k_B T} \kappa i_{app} = 0 \quad (11)$$

Therefore, we can know:

$$i_L(x) = \begin{cases} (C_{11} + C_{12}x)e^{\sqrt{\beta_1}x} + \frac{\kappa i_{app}}{\sigma_1 + \kappa}, & 0 \leq x < d_1 \\ (C_{21} + C_{22}x)e^{\sqrt{\beta_2}x} + \frac{\kappa i_{app}}{\sigma_2 + \kappa}, & d_1 < x \leq L \end{cases} \quad (12)$$

There are four undetermined coefficients in Eq. (12), and these coefficients cannot be determined according to the boundary conditions as depicted in Eq. (9). Additional boundary conditions at the interface of electrode regions 1 and 2 (see Fig. 3) are introduced as follows:

$$x = d_1, \quad i_L(x) = i_L(\text{known}), \quad \phi_L(x) = \phi_L(\text{known}) \quad (13)$$

Based on the a previous study on an acidic quinone RFB [9], the electrical resistance of a single-porosity electrode is formulated as:

$$r_{neg}^{DC} = \frac{d}{\sigma + \kappa} \left[1 + \frac{2 + \left(\frac{\sigma}{\kappa} + \frac{\kappa}{\sigma}\right) \cosh v}{v \sinh v} \right] \quad (14)$$

$$v = \sqrt{\frac{Fai_0 d^2}{RT} \left(\frac{1}{\kappa} + \frac{1}{\sigma} \right)} \quad (15)$$

The variable porosity electrode can be considered as a series of two single-porosity electrodes. The resistance with respect to the electrochemical overpotential is expressed as:

$$r_{net} = r_{net1} + r_{net2} \quad (16)$$

The flow resistance of the electrode has been defined in Eq. (2). Combining with Eqs. (3) and (4), the flow resistance can be further deduced as follows:

$$r_{flow} = \frac{\Delta PQ}{I_{app}^2} = \frac{\mu d}{A_{ed}} \left(\frac{Q}{I_{app}} \right)^2 \times \frac{\lambda_{CK}(1-\varepsilon)^2}{d_f^2 \varepsilon^3} \quad (17)$$

Thus the hydraulic resistance is expressed as:

$$r_{flow} = r_{flow1} + r_{flow2} \quad (18)$$

Combining Eqs. (13) and (15), the expression of the resistance function of the variable porosity electrode can be obtained as:

$$R_f = r_{net1} + r_{net2} + r_{flow1} + r_{flow2} = f(d_1, d_2, \varepsilon_1, \varepsilon_2) \quad (19)$$

Based on Eq. (16), the resistance of the variable porosity electrode is as a function of the specific length (area in the 2D model and volume in the 3D model) and porosity of the electrode material 1 and 2, which will affect the velocity distribution and the concentration distribution of active species within the electrode and thus the overall performance of the flow cell. In the future, the proposed 1D analytical model combined with certain mathematical optimization algorithms can obtain the optimal solution of local porosities.

3. RESULTS

3.1 Effects of the electrode thickness ratio

Based on Darcy's Law, the fluid velocity increases with increasing electrode porosity, that is, the average velocity of the electrolytes varies monotonously with the porosity thickness ratio that is defined as the ratio of the thickness of the layer with relatively larger porosity to the total thickness of the electrode. In addition, as mentioned in Section 2.1, in the present study, the porosities of the five layers of carbon paper sheets take

a pair of two porosity values (the porosity variations will be widened in the future). The larger porosity between the two values is implemented for the layer(s) near the membrane to match the relatively lower concentration of active species for the layers near the membrane. For example, the electrode thickness ratio of 0.8 corresponds to that the four layers of sheets near the membrane implements the higher porosity value while the layer near the flow field has the relatively low porosity.

The simulative results show that the average velocity has a maximum value with the change of the thickness ratio. For the porosity combinations of 0.7 and 0.82, 0.7 and 0.89, 0.82 and 0.89, the three combinations all get the maximum velocity when the thickness ratio of the layers with the relatively high porosity is 0.8. The thickness ratio for obtaining the maximum average velocity and its relationship with the porosity combinations and applied electrolyte flow rate need to be further explored.

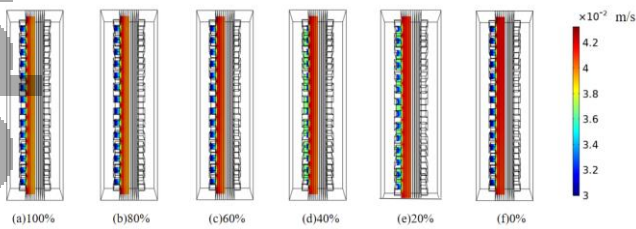


Fig 4 Velocity distribution variations with varying thickness ratios with $\varepsilon_1 = 0.89$, $\varepsilon_2 = 0.82$ (the thickness ratio defined as the ratio of the thickness of the layer with relatively larger porosity to the total thickness of the electrode).

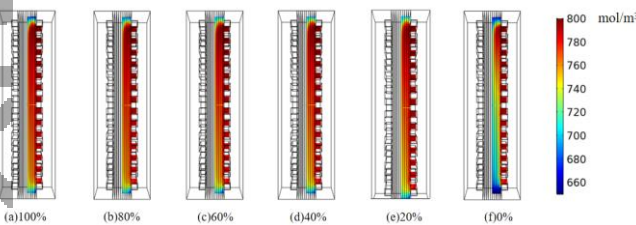


Fig 5 Variations of concentration distribution of reactants with varying thickness ratios with $\varepsilon_1 = 0.89$, $\varepsilon_2 = 0.82$ (the thickness ratio defined as the ratio of the thickness of the layer with relatively larger porosity to the total thickness of the electrode).

3.2 Effects of combinations porosities

According to the simulative results for the three groups of porosities (i.e., 0.7 and 0.82, 0.7 and 0.89, 0.82 and 0.89), the average velocity of electrolytes increases with increasing porosity differences in the porosity combinations. Among the current limited simulation results of electrode setups, when the porosity of the near-membrane 4 layers (corresponding the thickness ratio of 0.8) is 0.89 and the porosity of the near-flow-field layer is 0.7, the average velocity reaches the maximum.

3.3 Effects of anisotropic material

The isotropic assumption used in the present study is not satisfied in the model of the redox flow cell with the variable porosity electrode. However, within the scope of the respective electrode material, the isotropy assumption is regarded as applicable. Especially in the direction perpendicular to the membrane, physical properties such as porosity, permeability and conductivity in different layers and corresponding effects are assumed to be independent from each other, which are also reflected in the 1D analytical model. In this sense, the effects of the anisotropic material are taken into account by the isotropic assumption for two subsections of the electrode and extra boundary layer conditions applied at the interfaces between layers with different properties.

4. DISCUSSION

In the current version of the simulation model, it is assumed that the permeability of the electrode is isotropic, which may not be the case for certain materials that have distinct permeabilities in the in-plane and through-plane directions. The directional permeability values should be taken into account in the future study. In addition, the effects of the compression is also neglected in the present study, which should also be explored in the future. Last, the partition rule for dividing the electrode into the regions with different porosities should be extended to generate more complex shapes of regions or increase the total number of regions to further improve the overall efficiency of the redox flow cell, especially large-scale cell.

5. CONCLUSIONS

In the present study, the 3D, multi-physical vanadium redox flow battery model with the multi-layered electrode is devised, and a 1D analytical model for optimizing porosity distribution of multi-layered

electrode in the redox flow cell is proposed. The optimization results based on the 3D simulations are presented. Some of the main findings are as follows:

(1) The uniformity of electrolyte velocity and active-species concentration distributions is closely related to the porosity combination and the thickness ratio set for the multi-layered electrode.

(2) Under the case of the same porosity combination, the average velocity of the electrolyte increases first and then decreases when the thickness ratio of the electrode material with higher porosity increases from 0% to 100%.

ACKNOWLEDGEMENT

This work was supported by the National Undergraduate Training Program of Innovation and Entrepreneurship [201910335107].

REFERENCE

- [1] Aaron DS, Liu Q, Tang Z, Grim GM, Papandrew AB, Turhan A, Zawodzinski TA, Mench MM. Dramatic performance gains in vanadium redox flow batteries through modified cell architecture. *J. Power sources* 2012; 206:450-3.
- [2] Houser J, Clement J, Pezeshki A, Mench MM. Influence of architecture and material properties on vanadium redox flow battery performance. *J. Power Sources*. 2016; 302:369-77.
- [3] Chen W, Kang J, Shu Q, Zhang Y. Analysis of storage capacity and energy conversion on the performance of gradient and double-layered porous electrode in all-vanadium redox flow batteries. *Energy*. 2019; 180:341-55.
- [4] Yoon SJ, Kim S, Kim DK. Optimization of local porosity in the electrode as an advanced channel for all-vanadium redox flow battery. *Energy*. 2019 ;172:26-35.
- [5] Lölsberg J, Starck O, Stiefel S, Hereijgers J, Breugelmans T, Wessling M. 3D-printed electrodes with improved mass transport properties. *ChemElectroChem*. 2017; 4(12):3309-13.
- [6] Hereijgers J, Schalck J, Breugelmans T. Mass transfer and hydrodynamic characterization of structured 3D electrodes for electrochemistry. *Chemical Engineering Journal*. 2020; 384:123283.
- [7] Sun J, Zheng M, Luo Y, Yu Z. Three-dimensional detached serpentine flow field design for redox flow batteries. *J. Power Sources*. 2019; 428:136-45.
- [8] Tang A, Bao J, Skyllas-Kazacos M. Studies on pressure losses and flow rate optimization in vanadium redox flow battery. *J. Power Sources*. 2014 ;248:154-62.

- [9] Chen Q, Gerhardt MR, Aziz MJ. Dissection of the voltage losses of an acidic quinone redox flow battery. *J. Electrochem. Soc.* 2017 ;164(6):A1126.